Partial cross sections and photoelectron angular distributions in the region of the $4s \rightarrow 5p$ and $5s \rightarrow 6p$ resonances in krypton and xenon

M. G. Flemming, J-Z. Wu, and C. D. Caldwell
Department of Physics, University of Central Florida, Orlando, Florida 32816

M. O. Krause
Oak Ridge National Laboratory, Oak Ridge, Tennessee 37831
(Received 8 March 1991)

Using synchrotron radiation and photoelectron spectrometry, we have examined the $4s4p^6 5p$ resonance region in krypton and the $5s5p^6 6p$ resonance region in xenon. We have obtained partial and total cross sections, intensity ratios, and photoelectron angular distribution parameters for the energy regions 20.6–21.5 eV in xenon and 24.6–25.3 eV in krypton. We also report Shore parameters for all cross-section data taken. In addition to the anticipated single-electron transition, we clearly resolve features attributable to two-electron transitions in both species. Characteristics of these autoionizing states may differ considerably in the two available exit channels.

I. INTRODUCTION

There can be little argument that a significant portion of the development of atomic theory in recent decades has been stimulated by atomic photoionization measurements on the rare gases. As synchrotron radiation sources have provided photons at higher and higher resolution, and photoelectron spectrometry techniques have benefited from improvements in detection capabilities, experimental information has appeared that has stimulated new ways of looking at the old phenomenon of the photoelectric effect.

Of all the rare gases, xenon has been especially fruitful as a prototype system, serving as a source for analysis of autoionizing resonances between fine-structure components [1,2], behavior of s, p, and d subshell partial photoionization cross sections [3], and spin analysis of photoelectrons [4]. Theories invoking the relativistic random-phase approximation [5] and multiconfiguration quantum-defect theory [5,6] have been particularly successful in explaining the observed results of experiments designed to measure these various parameters.

Much attention has been given to the analysis of the behavior of the photoelectrons associated with the production of the $^2P_{1/2}$ and $^2P_{3/2}$ ions in both krypton and xenon. For example, Krause, Carlson, and Woodruff [7] give measurements for the angular distribution from 20 to 105 eV, and Wuilleumier *et al.* [8] give branching ratios for the two fine-structure components from 21 to 107 eV in Xe. Studies concentrating on the low energy behavior have been performed by Samson, Gardner, and Starace [9] for all the rare gases; Levinson, McGovern, and Gustafsson [10] give branching ratios, and Ederer [11] gives total cross sections for Xe. A more detailed look at the branching ratio and angular distribution at the $nsnp^6(n+1)p$ resonance, the first above the $^2P_{1/2}$ and $^2P_{3/2}$ ionization limits, has been given by Kemeny, Samson and Starace [12] and Codling *et al.* [13] for Xe and Ederer *et al.* [14] for both Xe and Kr.

One outstanding characteristic of photoionization of xenon in the region of the $5s \rightarrow 6p$ resonance is the presence of a number of two-electron excitations which lie near the principal single-electron transition. These transitions result from the promotion of two p electrons to pairs of the type sp, dp, sf, and df. A calculation reveals that there are 46 possible states of the type sp and dp which couple with the p^2 hole. However, only a number of these can be expected to have a measurable intensity. Earlier photoabsorption measurements [15,16] at high resolution confirm the existence of these transitions. Tentative assignments have been made [16] for some of the high-lying members of the series; no assignments exist for the possible states of the lower lying levels which we observe in this work.

Krypton, lying above xenon in the Periodic Table, has been the focus of less experimental activity [2,9,11,14,16]. Although the system can be expected to exhibit a structure similar to xenon, the splittings between the features are much smaller, making the details harder to observe. Nonetheless, a comparison between the transitions in the two species at the $ns \rightarrow (n+1)p$ resonance might be useful in attempting to make assignments to the various transitions.

Using the four-meter Normal Incidence Monochromator at the University of Wisconsin Synchrotron Radiation Center, together with an electron spectrometer, we have measured the photoelectron angular distributions and the intensity ratios corresponding to production of the $^2P_{1/2}$ and $^2P_{3/2}$ final states of xenon and krypton ions. In both cases we worked at 0.19-Å resolution and concentrated on the region around the $ns \rightarrow (n+1)p$ resonances, $4s \rightarrow 5p$ in krypton and $5s \rightarrow 6p$ in xenon. We also looked at some resonances in xenon with a higher resolution, 0.10 Å. We observe considerable differences in the behavior of the partial cross sections and of the photoelectron angular distributions in the two final-state channels

deriving from the presence of the single-electron transition and the two-electron transitions located in the same region.

II. EXPERIMENT

The electron spectrometer used in these experiments has been described in some detail in an earlier paper [17]. Briefly, it consists of three spherical sector plate electrostatic analyzers mounted on a platform that is free to rotate about the direction of the incoming radiation. Electrons are extracted from a source cell which is maintained at a constant gas pressure of approximately 10^{-4} Torr. All measurements, both of partial cross sections and angular distributions, were performed using two electron analyzers simultaneously. For the angular distributions one analyzer was placed at $\theta=0°$ and the second at $\theta=90°$ with respect to the electric field vector. Each analyzer was set to detect photoelectrons corresponding to the same fine-structure final state. The angular distribution parameter β is calculated from the ratio $r=I(0°)/I(90°)$ and the measured value of the polarization P of the incident radiation on the basis of the relations

$$I(\theta)\propto\frac{d\sigma}{d\Omega}=(\sigma/4\pi)[1+(\beta/4)(1+3P\cos(2\theta)] , \quad (1)$$

$$\beta=4(r-1)/[3P(r+1)-(r-1)] . \quad (2)$$

For the partial cross-section measurements two analyzers placed at 180° with respect to each other were used and the pair adjusted to lie at the "magic angle," $\theta_m=(1/2)\cos^{-1}[1/(3P)]$, at which the influence of β on the cross section is eliminated. Relative partial cross sections can be determined simultaneously by detecting photoelectrons corresponding to the $^2P_{1/2}$ final state in one analyzer and the $^2P_{3/2}$ final state in the other.

Measurements are made in both the photoelectron spectroscopy mode (PES) and the constant ionic state mode (CIS) [18]. The PES spectra allow us to determine the background and provide a series of independent measurements with which to normalize the CIS scans. In both Kr and Xe, the $^2P_{1/2}$ and $^2P_{3/2}$ components are clearly separated at a resolution $\Delta E/E=0.01$ for the analyzers and a pass energy of $E\approx 15$ eV. All final results are a composite of at least three independent spectra.

During the course of the experiments we worked at monochromator resolutions of 0.19 and 0.10 Å. As measurements at the higher resolution produced no additional features in the CIS spectra, most data were recorded at the lower resolution. The resolution of the monochromator was determined by a CIS scan over the ns' ($n=9$ to $n=11$) resonances lying between the $^2P_{3/2}$ and $^2P_{1/2}$ fine-structure levels in Xe^+. Values for the ns' widths were taken from a previous set of experiments [19].

The degree of polarization P of the ionizing radiation was determined by measurements of known values [20] of the photoelectron angular distribution parameter β for xenon, krypton, and argon at 21.22 eV. These same measurements, together with a determination of the photoelectron angular distribution from argon $^2P_{3/2}$ at 16.3 eV, where it is known [21] that $\beta=0$, served to determine the direction of the polarization vector and the asymmetry correction for the source volume as well. Polarization and asymmetry corrections were monitored periodically over the course of the measurements. The polarization was generally $P=0.78(2)$ during one experimental period, but was subject to larger changes during another period, with $P=0.65$ a minimum value. Appropriate corrections were applied to the data.

III. RESULTS AND DISCUSSION

A. Xenon

In Fig. 1(a) are shown the results for the partial and total cross sections for the production of the two final states of the Xe^+ ion $5s^25p^5(^2P_{1/2,3/2})$. The labels 1–9 for the features given at the top of the graph coincide with those used by Codling and Madden [16]. The energy scale of the data was shifted by a constant value calculated from the deviation of the energy of a peak in the *fitted* total cross section (see Sec. IV) from the corresponding peak energy given by these authors. For the lower section of the spectrum, peaks 1–5, this was resonance labeled 3 at 20.952 eV and for the upper section, peaks 6–9, resonance labeled 7 at 21.336 eV.

PES spectra that contained both fine-structure components were used to calculate intensity ratios at individual points. The relative partial cross sections obtained by CIS scans were normalized to each other using the PES ratios measured at the end points of the scans, with the other values serving as checks. These partial cross sections were added together to form the relative total cross section. The relative total cross section was converted to an absolute total cross section by first fitting the data to Shore profiles (see Sec. IV) to determine the resonance effects at the end points, then normalizing these values at the end points to a continuum determined from data given by West and Morton [22], namely, at 20.32 eV (32.71 Mb) and 22.14 eV (25.24 Mb). The upper and lower sections of the spectra were treated separately but normalized to the same absolute cross sections from the values given above.

As can be seen, there are at least nine spectral features visible in both the $J=1/2$ and $J=3/2$ channels. Feature 3, at 20.952 eV, has been assigned to the single-electron transition $5s^25p^6\rightarrow 5s5p^66p$ by Codling and Madden [16]. The remainder has been primarily attributed to two-electron transitions of the type $5p^6\rightarrow 5p^4nln'l'$, with nl and $n'l'$ most likely to be $5d$ and $6p$ orbitals.

As was already observed by Codling and Madden, the excitations appear in the total cross section primarily as "window" resonances. They are, for the most part, symmetric in shape, although resonances 2 and 9 appear more asymmetric. Resonance 6, which was observed in the total cross section as a very weak window, is seen to display strong excursions when contributions are separated into the $J=1/2$ and $J=3/2$ channels. The behavior of resonances 2 and 9 is very similar in the two exit channels, but differs from that of the other resonances, which suggests that these features belong to the same $nln'l'$ series, possibly the $5d6p$ and $6d6p$ two-electron transi-

tions. Codling and Madden chose resonance 3 as one of the $J=1$ single-electron transitions due to the great similarity of its profile to that of the following members of the series. While the second $J=1$ single-electron transition has not been clearly identified, they thought it likely to be resonance 1 or 2. However, by comparing the similarities of the partial cross sections and the asymmetry parameter in the two exit channels, it is possible that a more likely choice would be resonance 4.

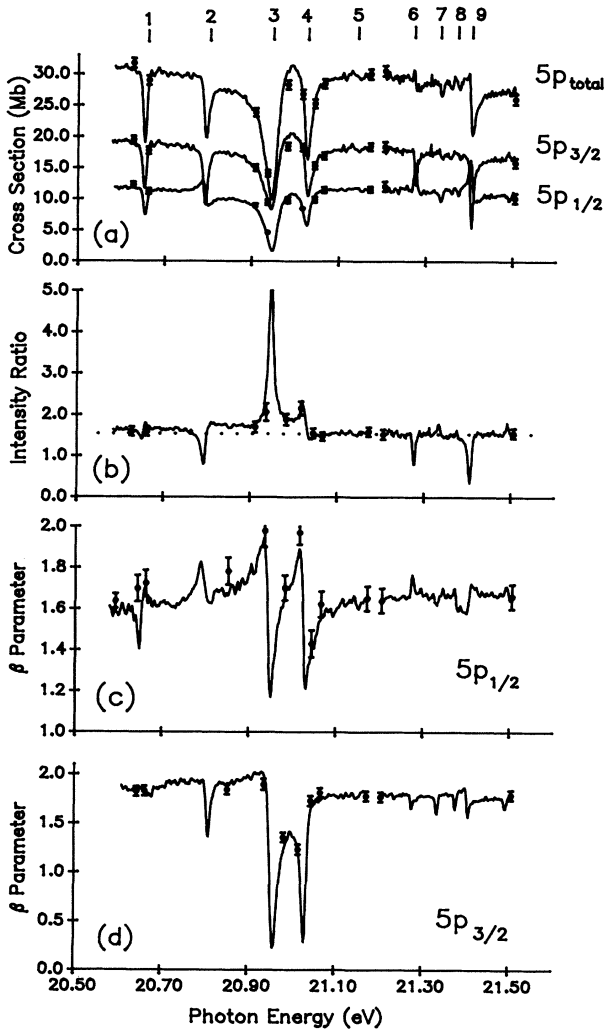

FIG. 1. Photoionization in the vicinity of the $5s5p^6 6p$ resonance in xenon. Measurements were taken in the CIS mode with a step size (2 meV) that was less than the 7-meV optical resolution. Labels are taken from Ref. 16. (a) Partial and total cross sections. The experimental data have been converted to absolute values by normalization to the measurement of the total cross section by West and Morton (Ref. 22). (b) Intensity ratio $R=\sigma(3/2)/\sigma(1/2)$. The solid line is the result of the CIS measurement, and the individual points with error bars are results of PES measurements. The dotted line at $R=1.54$ is the continuum result quoted by Samson, Gardner, and Starace [9]. (c) Photoelectron angular distribution parameter β for the $J=1/2$ fine-structure component. (d) Photoelectron asymmetry parameter β for the $J=3/2$ fine-structure component.

Figure 1(b) shows the intensity ratio $R=\sigma(3/2)/\sigma(1/2)$, where $\sigma(3/2)$ and $\sigma(1/2)$ are the partial cross sections for the production of the $^2P_{3/2}$ and $^2P_{1/2}$ states, respectively. The continuum intensity ratio, $R=1.59(7)$, is in good agreement with the value of 1.54 obtained by Samson, Gardner, and Starace [9]. Transition 3 shows the most marked deviation from the value at the continuum, with a maximum of $R=4.8$ at the peak. This result is notably less than the semiempirical result of 8.8 ± 0.5 calculated by Kemeny, Samson, and Starace [12]. Codling *et al.* [13] measured an average maximum value of 2.6 at a resolution of 0.5 Å. In our measurements the effect of the 0.19-Å bandpass on the two partial cross-section widths at this particular resonance is small. Using the results of the Shore fits, we obtain an unconvoluted ratio of $R=5.4$ at the maximum. If we convolute our fit results with a Gaussian slit function of 0.5 Å, as used in Ref. 13, the value at the peak becomes 3.4, which is in satisfactory accord with their measured ratio of 2.6.

Although not as pronounced, all transitions except 5 and 8 show some structure in the intensity ratio. Transitions 2 and 9 show as much similarity in structure in R as they did in the partial cross sections. Transition 4 is seen as the only other transition to show an increase in intensity ratio as did the single-electron transition, 3. This adds weight to the possibility of transition 4 being the other spin-orbit component of the single-electron excitation.

Figures 1*c* and 1*d* show the measured photoelectron angular distributions. As was theorized by Dill [23], there is a rapid fluctuation in β across the autoionizing resonances. The single-electron transition, 3, and transition 4 have intense fluctuations when compared with the other transitions. As the variation in 4 is as strong as that in 3, and, in addition, displays a similar character, this lends support to the suggestion that transition 4 may be the second spin-orbit component of the single-electron excitation. The off-resonance values for β of 1.55(6) for the $^2P_{1/2}$ component and 1.65(5) for the $^2P_{3/2}$ component at 21.22 eV are in good agreement with previous experiments, such as those of Krause, Carlson, and Woodruff [7] ($\beta=1.57$ and $\beta=1.72$, respectively) and Codling *et al.* [13].

B. Krypton

The partial and total relative cross sections for the production of the two final states of the Kr^+ ion $4s^24p^5(^2P_{1/2,3/2})$ were obtained in the same manner as those for xenon. Data were converted to an absolute cross section by normalization to the total cross section continuum values interpolated from the results of Marr and West [24] at 24.31 eV (29.3 Mb) and 25.83 eV (25.8 Mb). The labels 1–6 for the features given at the top of the graph coincide with those of Codling and Madden [16]. The energy scale of the data was shifted so as to adjust the value of resonance 4 to 24.952 eV, as obtained by these authors.

From the graph in Fig. 2(a) we can distinguish at least six spectral features in the $J=1/2$ and $J=3/2$ channels. As was the case for xenon, the resonances appear in the total cross section as window resonances. They too are, for the most part, symmetric, except for resonances 1 and 6. Resonance 2, appearing in the total cross section as a very weak "window," is seen to be much stronger in each individual decay channel. Codling and Madden assigned features 3 and 5, at 24.922 and 24.993 eV, respectively, to the strong single-electron transitions of the predominant series $4s^2 4p^6 \rightarrow 4s 4p^6 5p$. The remainder has been attributed to the two-electron transitions of the type $4p^6 \rightarrow 4p^4 nln'l'$, with nl and $n'l'$ most likely to be $4d$ and $5p$ orbitals. It should be noted, however, that transition 4, tentatively labeled a two-electron transition, shows a markedly more intense response in the $J=1/2$ exit channel than any other transition, more compatible with a single-electron transition than feature 5.

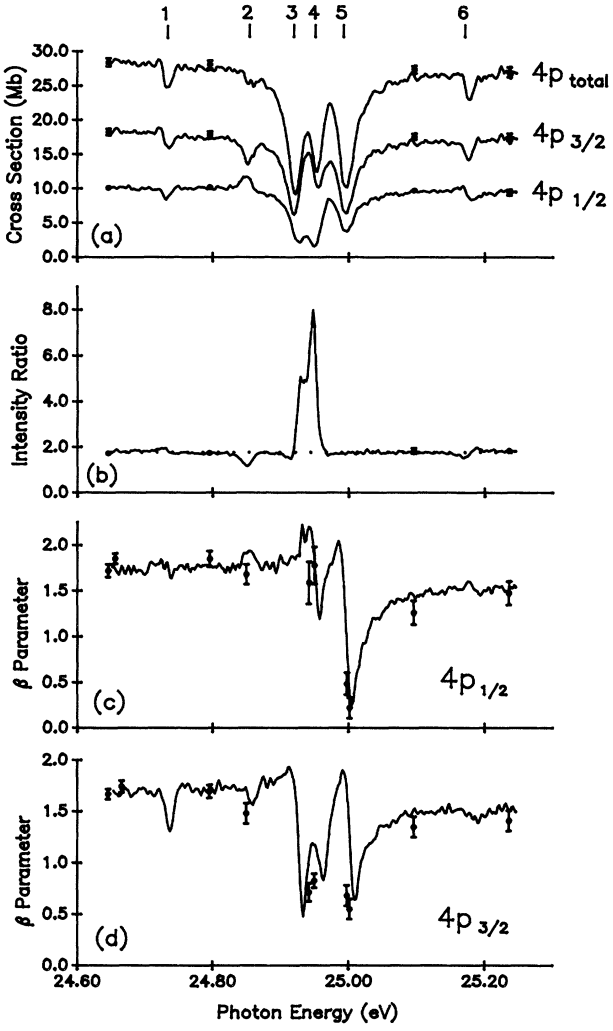

FIG. 2. Photoionization in the vicinity of the $4s5p^6 5p$ resonance of krypton. Measurements were taken in the CIS mode with a step size (2 meV) that was less than the 10-meV optical resolution. Labels are taken from Ref. 16. (a) Partial and total cross sections. The experimental results have been converted to absolute values by normalization to the values for the total cross section given by Marr and West [24]. (b) Intensity ratio $R=\sigma(3/2)/\sigma(1/2)$. The solid line is the result of the CIS measurement, and the individual points with error bars are results of PES measurements. The dotted line at $R=1.77$ is the continuum result quoted by Samson, Gardner, and Starace [9]. (c) Photoelectron angular distribution parameter β for the $J=1/2$ fine-structure component. (d) Photoelectron angular distribution parameter β for the $J=3/2$ fine-structure component.

Apart from transitions 3 and 4, the intensity ratio, shown in Fig. 2(b), varies little across the region of the spectrum that we have studied. Some indications of transitions 2 and 6 are seen in the ratio, but this reflects more the very different line shapes than it does a profound change in the intensity ratio. Outside of the resonance region we obtain a value $R=1.76(7)$. This is in good agreement with the value of $R=1.77$ obtained by Samson, Gardner, and Starace [9]. At the maximum, resonance 4, we obtain a value of $R=8.0$. This is much larger than was obtained at the same energy by Ederer *et al.* [14]. This difference may be attributed to the enhanced resolution of our experiment. Calculating the intensity ratio using the Shore results, we obtain an unconvoluted value of 18.3 at the maximum. This large ratio is partially due to the dissimilar structure of the two exit channel resonances. If the intensity ratio is compared to the xenon data, one would expect transitions 3 and 5 to have strong peaks with a smaller peak at transition 4. Instead, transition 4 has the strongest response. Transition 3 is only half the size of transition 4, and 5 shows the same response as the other two-electron transitions. Thus, the intensity ratio alone suggests that 3 and 4 are the single-electron transitions, and 5 is a strong two-electron transition.

In Figs. 2(c) and 2(d) are shown the photoelectron angular distributions. Once again rapid fluctuations in β were observed across the resonances. In the $J=3/2$ channel, transitions 3 and 5 show the strongest excursions. Transition 4 has a slightly less intense variation but, as in xenon, is markedly more pronounced than the other two-electron transitions. In the $J=1/2$ channel transitions 4 and 5 show the most intense fluctuation, with 5 having the highest response. Transition 3 has a much reduced fluctuation and does not have the same type of response as seen in xenon. Thus, while the similar behavior in the cross sections suggested that 3 and 4 might be the two single-electron transitions, this is not supported by a corresponding similarity in the behavior of β.

IV. PARAMETRIZATION

A line-shape fit of the autoionizing resonances has several advantages. Instead of listing a long table of numbers, a much shorter table of the parameters for the line-shape equation can be given which allows a faithful reproduction of the original data. The parameters also provide a numerical means with which to compare reso-

nances within the same system and between different systems. Because the region of observation includes many overlapping features, the parametrization scheme developed by Shore [25] was selected as the most convenient. Within this scheme the line shape is given by the expression

$$\sigma(E)=C(E)+\sum_i \frac{(E-E_i)(\Gamma_i/2)a_i+(\Gamma_i/2)^2 b_i}{(E-E_i)^2+(\Gamma_i/2)^2} .$$

The parameters E_i and Γ_i are, for the ith resonance, the peak energy and peak width at half the maximum value [full width at half maximum (FWHM)], respectively. Parameters a_i and b_i are proportional to products of dipole and Coulomb matrix elements, and $C(E)$ is the continuum contribution. All three have dimensions of cross section. $C(E)$ is assumed to vary linearly with energy, and a_i and b_i are assumed constant in energy across each resonance.

The method used to optimize the Shore parameters to the real data has been outlined by Bevington [26]. The procedure performs a least-squares fit by a combination of linearization of the fitting function and gradient search method. An added complication to the fitting procedure was the necessity of removing the effect of the monochromator bandpass. This was done by convoluting the line shape calculated on the basis of the assumed Shore parameters with the slit function before comparing to the real data. The slit function used here was a normalized Gaussian curve with a FWHM equal to the measured bandpass. The final numbers quoted are the Shore parameters for the natural resonance structure which, when convoluted with the slit function, reproduce the experimental data.

The Shore parameters obtained from fitting the xenon and krypton data shown in Figs. 1(a) and 2(a), respectively, are listed in Table I for the total cross sections and Table II for the partial cross sections. Table I also lists values obtained by Ederer [11] from similar measurements, converted from attenuation lengths to Mb. The continuum contributions were obtained by performing a linear interpolation of the cross-section data used to normalize the experimental results to absolute cross sections, as described in Sec. III. These contributions are given by

$$C(E)=116.103\ \text{Mb}-(4.104\ \text{Mb/eV})E$$

for Xe in Table I ,

$$C(E)=85.277\ \text{Mb}-(2.303\ \text{Mb/eV})E$$

for Kr in Table I ,

$$C(E)=46.17\ \text{Mb}-(1.63\ \text{Mb/eV})E$$

for Xe $5p_{1/2}$ in Table II ,

$$C(E)=69.93\ \text{Mb}-(2.47\ \text{Mb/eV})\text{E}$$

for Xe $5p_{3/2}$ in Table II ,

TABLE I. Shore parameters for total cross section.

	This work[a]				Ederer[b]			
Code	E_p (eV)[c]	Γ (meV)	a (Mb)	b (Mb)	E_p (eV)	Γ (meV)	a (Mb)	b (Mb)
				Xe $5p$				
1	20.654[−9]	5.8	−0.76	−17.70	20.664	3.7	1.86	−20.45
2	20.794[−6]	11.0	−3.90	−11.03	20.805	8.1	−5.02	−10.04
3	20.952[d]	34.8	12.64	−18.57	20.951	31.2	8.37	−18.04
4	21.027[−4]	19.7	−4.12	−15.41	21.030	14.6	−4.09	−13.02
6	21.277[+1]	9.9	−2.30	−1.03				
7	21.337[+1]	5.8	0.32	−3.19				
7′	21.360	7.2	0.81	−2.40				
8	21.373[−4]	11.7	−2.37	−0.98				
9	21.405[−3]	8.4	−9.26	−6.02	21.407	5.8	−8.74	−8.55
				Kr $4p$				
1	24.732[−4]	4.9	−2.41	−7.27	24.735	4.0	−4.28	−9.67
2	24.857[+2]	12.0	0.21	−1.92				
3	24.924[+2]	22.6	9.04	−19.03		19.0	10.41	−16.73
4	24.952[d]	21.7	−1.32	−18.77		7.5	0.00	−18.59
5	24.992[−1]	26.0	−9.83	−17.20	24.992	22.8	−11.16	−15.99
6	25.177[+3]	5.7	−0.91	−7.30	25.173	3.9	−2.23	−10.97

[a]The uncertainties associated with the fit itself are $E_p, \Gamma \pm 0.004$ eV; $a, b \pm 1.0$ Mb. All parameters are also subject to a systematic error due to the uncertainty in the width of the slit function, 0.19 Å±0.02 for krypton and peaks 1–4 in xenon, 0.10 Å±0.02 for peaks 6–9 in xenon.

[b]Reference [11].

[c]Numbers given in brackets are the deviations of the fitted energies from the corresponding spectroscopic values reported in Ref. [16].

[d]Reference value.

$C(E)=29.76$ Mb$-(0.80$ Mb/eV$)E$

for Kr $4p_{1/2}$ inTable II ,

$C(E)=55.52$ Mb$-(1.50$ Mb/eV$)E$

for Kr $4p_{3/2}$ in Table II .

$C(E)$ is in Mb, E in eV. The fitted energies E_p in Table I are referenced to the measured energies of peak 3 for xenon and peak 4 for krypton obtained by Codling and Madden [16]. The numbers given in brackets are the deviations of the fitted energies from the corresponding spectroscopic values for the remaining features. A comparison of the convoluted fit with the measured data is shown in Figs. 3 and 4.

By comparing Ederer's results [11] to our own, we see that our widths are consistently larger. This includes widths that were wide enough to have experienced little bandpass broadening. The a and b values all have the

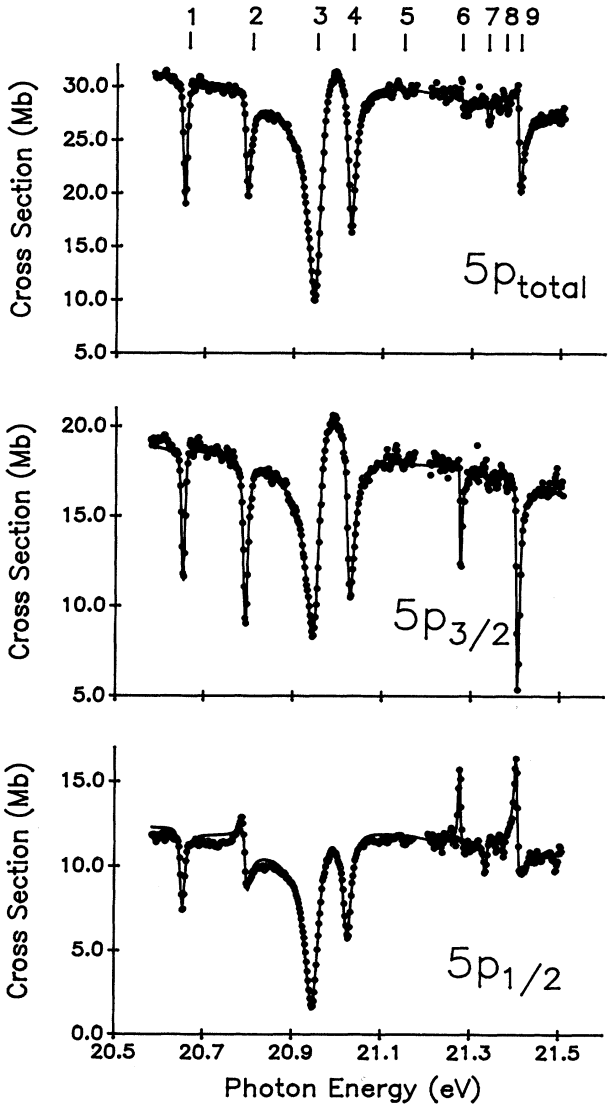

FIG. 3. Shore fit of xenon cross-section data. The solid line is data created from the Shore equation using the values listed in Tables I and II, convoluted with a bandpass of 0.19 Å for the lower section and 0.10 Å for the upper section. Experimental data are represented by points.

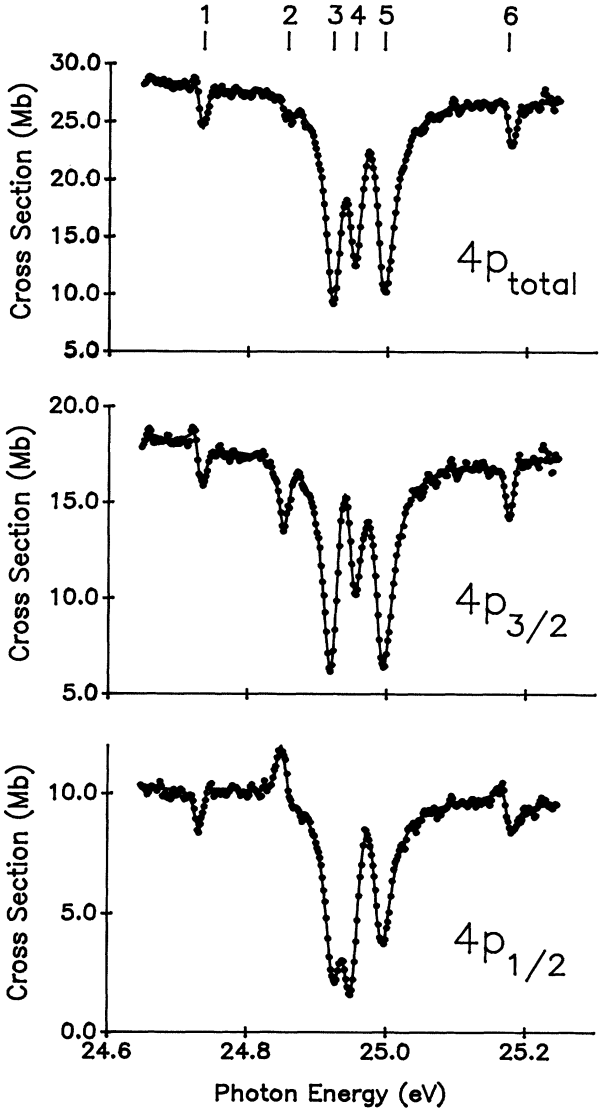

FIG. 4. Shore fit of krypton cross-section data. The solid line is data created from the Shore equation using the values listed in Tables I and II, convoluted with a bandpass of 0.19 Å. Experimental data are represented by points.

TABLE II. Shore parameters for individual fine-structure channels.[a]

Code	E_p (eV)	Γ (meV)	a (Mb)	b (Mb)	E_p (eV)	Γ (meV)	a (Mb)	b (Mb)
		Xe $5p_{1/2}$				Xe $5p_{3/2}$		
1	20.654	10.2	−1.31	−5.31	20.654	4.1	1.71	−13.30
2	20.800	10.6	−3.48	−2.19	20.794	8.4	−1.08	−11.69
3	20.952	37.7	5.02	−9.28	20.952	31.9	7.86	−9.23
4	21.026	23.2	0.28	−6.63	21.027	17.5	−5.00	−8.74
5								
6	21.277	3.7	−1.79	6.22	21.276	3.2	−4.06	−8.12
7	21.336	7.2	0.77	−2.08	21.336	4.9	−1.37	−0.92
7′	21.357	<0.2	−35.74	−16.70	21.355	4.7	−0.69	−0.94
8	21.376	4.9	−0.33	−1.66	21.375	0.4	−11.59	−4.21
9	21.407	7.1	−6.11	4.36	21.405	7.0	−4.50	−12.69
		Kr $4p_{1/2}$				Kr $4p_{3/2}$		
1	24.733	7.4	0.67	−2.62	24.731	3.4	−4.73	−4.40
2	24.850	9.7	−0.64	3.18	24.853	11.6	0.72	−4.46
3	24.927	19.7	2.25	−6.46	24.923	22.1	7.39	−12.77
4	24.952	25.3	2.46	−9.67	24.952	19.5	−4.07	−9.59
5	24.990	26.8	−4.63	−6.08	24.992	25.8	−5.39	−11.04
6	25.177	6.8	−2.27	−1.70	25.177	5.9	1.77	−5.17

[a]The uncertainties associated with the fit itself are $E_p, \Gamma \pm 0.004$ eV; $a, b \pm 1.0$ Mb. All parameters are also subject to a systematic error due to the uncertainty in the width of the slit function, 0.19 Å±0.02 for krypton and peaks 1–4 in xenon, 0.10 Å±0.02 for peaks 6–9 in xenon.

same order of magnitude as those of Ederer. The sign of a, which determines the side of the resonance on which destructive interference occurs, is the same for all peaks listed, except peak 1 in xenon and peak 4 in krypton. However, the magnitudes of a for these latter two features, which control the degree of asymmetry, are so small that a difference in sign would have little effect. It should be noted that the width of peak 4 in Kr is given as three times the value quoted by Ederer. However, by comparing this peak to the resonances on either side in Fig. 2(a), and to Fig. 1a in Ederer's work, it is apparent that the width we obtained from our fit is reasonable.

Resonance 5 of Xe, shown in Fig. 3, is not listed in the tables because the structure demonstrated so small a deviation from the continuum that fitting this peak yielded dubious results. It was determined, however, that the width of the peak, approximately 0.2 meV, was small enough not to have influenced the resonances next to it by an appreciable amount. Thus the numbers should be reliable even without including this peak in the fit. In xenon, Tables I and II, there is a peak that we have designated as feature 7′. This feature, which was not seen by Codling and Madden [16], was fitted for completeness.

The fit shown for the $^2P_{1/2}$ exit channel in Fig. 3 deviates slightly from the data in the lower energy region, specifically between peaks 1 and 2. This may be due to the presence of one broad or many small peaks that were not included in the fit. If missing peaks were to be represented by an additional peak, the fit would improve. However, this was not done because there is no real evidence of the existence of extra features from any source other than from the fit itself.

As was the case for xenon, the fitting-convolution procedure applied to krypton satisfactorily reproduces the spectral data in both exit channels and the total cross section. This is shown in Fig. 4. There are weak indications for additional minor transitions between peaks 1 and 2 and between peaks 5 and 6.

V. CONCLUSION

In this work the autoionization features near the $4s \rightarrow 5p$ excitation in krypton and the corresponding $5s \rightarrow 6p$ excitation in xenon were studied in the two exit channels, $^2P_{3/2}$ and $^2P_{1/2}$, by measuring both the partial cross sections $\sigma_{3/2}$ and $\sigma_{1/2}$ and the photoelectron angular distribution parameters, $\beta_{3/2}$ and $\beta_{1/2}$. This is the most complete data set obtained to date for these autoionization transitions and the nearby two-electron transitions of the type $p^2 \rightarrow nln'l'$. The advantage of using emission studies as opposed to absorption studies in these measurements is clearly seen in the appearance of features that have entirely opposite behavior in the two exit channels, resulting in a cancellation in the absorption spectrum.

Our emission data, recorded at a resolution approaching the best resolution reported for absorption data, allowed us to draw a number of parallels between certain two-electron transitions in krypton and xenon. Accurate natural widths, and other characteristic parameters, were obtained for all the observed resonances in both exit channels by applying a Shore parameter fitting procedure to our data.

The confusion generated by the behavior of transition 4 in both xenon and krypton, and transition 5 in krypton, makes even a tentative assignment of the resonances difficult. With the breakdown of *LS* coupling and the presence of presumably strong configuration interaction in both systems, any kind of standard energy-level or cross-section calculation for these systems is extremely difficult. It is hoped that with our new detailed data, more theoretical work may be done to better understand these systems.

ACKNOWLEDGMENTS

This research was supported by the National Science Foundation under Grant Nos. NSF-PHY-8701193 and NSF-PHY-8707750. M.O.K. acknowledges support by the Division of Chemical Sciences, U.S. Department of Energy under Contract No. DE-AC05-84OR21400 with Martin Marietta Energy Systems, Inc. The University of Wisconsin Synchrotron Radiation Center is operated under NSF Grant No. DMR-8821625.

[1] J. A. R. Samson and J. L. Gardner, Phys. Rev. Lett. **31**, 1327 (1973).
[2] Y. Morioka, M. Watanabe, T. Akahori, A. Yagishita, and M. Nakamura, J. Phys. B **18**, 71 (1985).
[3] J. B. West, P. R. Woodruff, K. Codling, and R. G. Houlgate, J. Phys. B **9**, 407 (1976).
[4] C. Heckenkamp, F. Schäfers, G. Schönhense, and U. Heinzmann, Z. Phys. D **2**, 257 (1986).
[5] W. R. Johnson, and K. T. Cheng, Phys. Rev. A **20**, 978 (1979); W. R. Johnson, K. T. Cheng, K-N. Huang, and M. Le Dourneuf, *ibid.* **22**, 989 (1980).
[6] J. Geiger, Z. Phys. A **282**, 129 (1977).
[7] M. O. Krause, T. A. Carlson, and P. R. Woodruff, Phys. Rev. A **24**, 1374 (1981).
[8] F. Wuilleumier, M. Y. Adam, P. Dhez, N. Sandner, V. Schmidt, and W. Mehlhorn, Phys. Rev. A **16**, 646 (1977).
[9] J. A. R. Samson, J. L. Gardner, and A. F. Starace, Phys. Rev. A **12**, 1459 (1975).
[10] H. J. Levinson, I. T. McGovern, and T. Gustafsson, J. Phys. B **13**, 253 (1980).
[11] D. L. Ederer, Phys. Rev. A **4**, 2263 (1971); **14**, 1936 (1976).
[12] P. C. Kemeny, J. A. R. Samson, and A. F. Starace, J. Phys. B **10**, L201 (1977).
[13] K. Codling, J. B. West, A. C. Parr, J. L. Dehmer, and R. L. Stockbauer, J. Phys. B **13**, L693 (1980).
[14] D. L. Ederer, A. C. Parr, J. B. West, D. Holland, and J. L. Dehmer, Phys. Rev. A **25**, 2006 (1982).
[15] K. Codling and R. P. Madden, Phys. Rev. A **4**, 2261 (1971).
[16] K. Codling and R. P. Madden, J. Res. Nat. Bur. Std. Sec. A **76a**, 1 (1972).
[17] M. O. Krause, T. A. Carlson, and A. Fahlman, Phys. Rev. A **30**, 1316 (1984).
[18] M. O. Krause, F. Cerrina, and A. Fahlman, Phys. Rev. A **50**, 1118 (1983).
[19] J-Z. Wu, S. B. Whitfield, C. D. Caldwell, M. O. Krause, P. van der Meulen, and A. Fahlman, Phys. Rev. A **42**, 1350 (1990).
[20] J. Kreile and A. Schweig, J. Elec. Spectrosc. Relat. Phenom. **20**, 191 (1980).
[21] M. O. Krause, in *Synchrotron Radiation Research,* edited by H. Winick and S. Doniach (Plenum, New York, 1980), Chap. 5.
[22] J. B. West and J. Morton, At. Data **22**, 103 (1978).
[23] D. Dill, Phys. Rev. A **7**, 1976 (1973).
[24] G. V. Marr and J. B. West, At. Data and Nucl. Data Tables Vol. **18**, 497 (1976).
[25] B. W. Shore, J. Opt. Soc. Am. **57**, 881 (1967).
[26] P. R. Bevington, *Data Reduction and Error Analysis for the Physical Sciences* (McGraw-Hill, New York, 1969).